

# Long-range order and thermal stability of thin $\text{Co}_2\text{FeSi}$ films on $\text{GaAs}(111)\text{B}$

B. Jenichen,\* J. Herfort, K. Kumakura,<sup>†</sup> and A. Trampert

*Paul-Drude-Institut fuer Festkoerperelektronik, Hausvogteiplatz 5-7, D-10117 Berlin, Germany*

(Dated: January 11, 2022)

$\text{Co}_2\text{FeSi}/\text{GaAs}(111)\text{B}$  hybrid structures are grown by molecular-beam epitaxy and characterized by transmission electron microscopy (TEM) and x-ray diffraction. The  $\text{Co}_2\text{FeSi}$  films grow in an island growth mode at substrate temperatures  $T_S$  between  $T_S = 100^\circ\text{C}$  and  $425^\circ\text{C}$ . The structures have a stable interface up to  $T_S = 275^\circ\text{C}$ . The films contain fully ordered  $L_{21}$  and partially ordered  $B2$  phases. The spatial distribution of long-range order in  $\text{Co}_2\text{FeSi}$  is characterized using a comparison of TEM images taken with superlattice reflections and the corresponding fundamental reflections. The spatial inhomogeneities of long-range order can be explained by local non-stoichiometry due to lateral segregation or stress relaxation without formation of extended defects.

PACS numbers: 75.50.Bb, 81.15.Hi, 61.05.J-, 68.35.Ct

## I. INTRODUCTION

There is an increasing interest in Heusler alloys as candidates for sources of spin injection into semiconductors [1–4]. The Heusler alloy  $\text{Co}_2\text{FeSi}$  is a ferromagnetic half-metal with a Curie temperature larger than 1100 K [5, 6]. The lattice parameter matches that of GaAs. Therefore,  $\text{Co}_2\text{FeSi}$  is a suitable material for spin injection into GaAs-based structures such as for example spin light-emitting diodes (spin-LEDs [7–10]) and spin field effect transistors [11]. Samples produced by radio frequency magnetron sputtering have shown magnetically dead layers near the interfaces [12]. An epitaxial growth technique like molecular-beam epitaxy (MBE) may overcome these difficulties.

Recent theoretical studies indicate that a  $\{111\}$  interface may be superior to  $\{001\}$  interfaces [13] with respect to the half-metallic properties of  $\text{Co}_2\text{FeSi}$ . Moreover, reacted compounds sometimes developing during  $\text{Co}_2\text{FeSi}$  growth on  $\text{GaAs}(001)$  are bounded by  $\{111\}$  planes [14]. This observation led to the hypothesis that a  $\{111\}$  interface would be more stable. At the same time, reduced diffusion is expected perpendicular to the interface during growth on  $\text{GaAs}(111)\text{B}$ .

X-ray and electron diffraction experiments yield information about structure and long-range order of Heusler alloys and related materials [6, 15–18]. In this study MBE grown  $\text{Co}_2\text{FeSi}/\text{GaAs}(111)\text{B}$  hybrid structures are investigated by transmission electron microscopy (TEM), x-ray diffraction and atomic force microscopy (AFM) in order to characterize the structural properties and the stability of the ferromagnet/semiconductor (FM/SC) interface and the  $\text{Co}_2\text{FeSi}$  film. The growth mode of the epitaxial film [19–22] is expected to have a fundamental influence on its structural properties.

## II. EXPERIMENTAL

The structures were grown by solid-source MBE. The growth procedure on  $\text{GaAs}(001)$  is described in detail in Refs. [23, 24]. In our case  $\text{GaAs}(111)\text{B}$  samples with a 50-nm-thick GaAs buffer layer and an As-stabilized,  $(2\times 2)$ -reconstructed surface were grown first on a  $\text{GaAs}(111)\text{B}$  substrate and then transferred to an As-free growth chamber, in which stoichiometric  $\text{Co}_2\text{FeSi}$

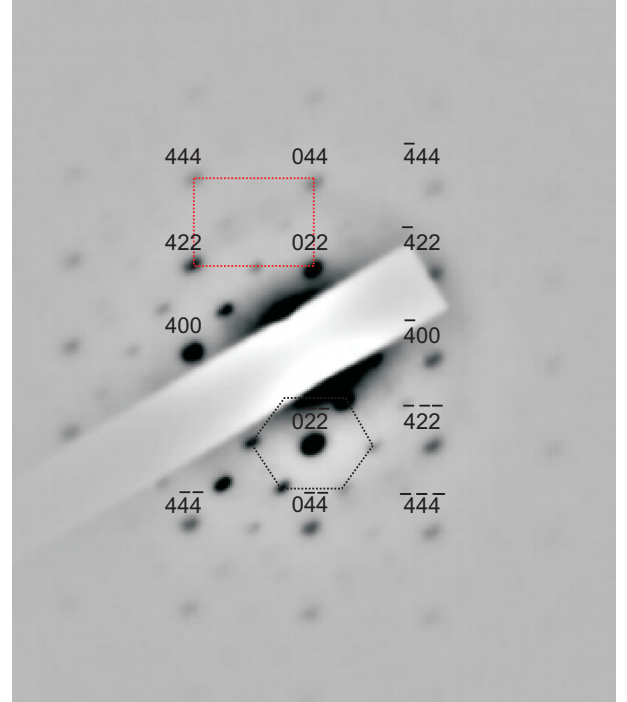


Figure 1. Selected area diffraction pattern along the  $\text{Co}_2\text{FeSi}/\text{GaAs}$   $[01\bar{1}]$  zone axis of a sample grown at  $T_S = 275^\circ\text{C}$ . A rectangular pattern of  $\text{Co}_2\text{FeSi}$  fundamental reflections (indexed, red dashed line) of the  $L_{21}$  structure is observed. This rectangular pattern is slightly more pronounced than the hexagonal pattern (black dashed line) of the superlattice maxima in the vicinity.

\* bernd.jenichen@pdi-berlin.de

<sup>†</sup> Also at NTT Basic Research Laboratories, 3-1 Morinosato Wakamiya, Atsugi-shi, Kanagawa 243-0198, Japan.

films were grown on top for different substrate temperatures  $T_S$  ranging between  $T_S = 100^\circ\text{C}$  and  $425^\circ\text{C}$ . Co, Fe, and Si are co-deposited from high-temperature effusion cells. The evaporation rates are controlled by the cell temperatures and are in accordance with the optimized fluxes for the growth of stoichiometric  $\text{Co}_2\text{FeSi}$  films on GaAs(001) substrates [23]. The growth rate was approximately one monolayer in three minutes. The base pressure was about  $1 \times 10^{-10}$  Torr. The growth was monitored by *in-situ* reflection high energy electron diffraction (RHEED). The samples were investigated by dark-field and high-resolution (HR) TEM. For that purpose cross-sectional TEM specimens were prepared by mechanical lapping and polishing, followed by argon ion milling according to standard techniques. TEM images were acquired with a JEOL 3010 microscope operating at 300 kV. In addition, X-ray measurements of diffraction and reflectivity were performed in a Panalytical X'Pert diffractometer equipped with a Ge 220 Hybrid monochromator using  $\text{CuK}\alpha_1$  radiation. Some of the samples were characterized by *ex-situ* AFM almost immediately after the growth. A Digital Instrument Nanoscope was utilized for this purpose. Depth profiles of the film constituents inside the GaAs buffer layer were determined by secondary ion mass spectrometry (SIMS). The  $\text{Co}_2\text{FeSi}$  layer was removed by selective wet chemical etching prior the SIMS profiling. The SIMS measurements were performed with a CAMECA IMS4F system.

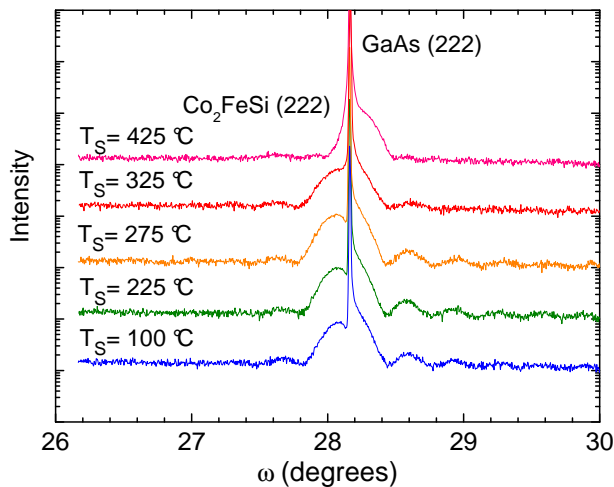


Figure 2. High resolution x-ray diffraction curves measured near the GaAs 222 reflection of samples grown at different substrate temperatures  $T_S$ . The narrow peak is the quasi-forbidden GaAs reflection and the broader maximum is the  $\text{Co}_2\text{FeSi}$  222 superlattice reflection indicating at least a  $B2$  ordering of all the films. The thickness fringes demonstrate a high quality of the FM/SC interface and surface.

### III. RESULTS

Fully ordered  $\text{Co}_2\text{FeSi}$  crystallizes into the face centered  $L2_1$  structure. This structure can be viewed as an fcc lattice with a basis consisting of four atoms A, B, C, and D with coordinates A(0, 0, 0), B(0.25, 0.25, 0.25), C(0.5, 0.5, 0.5), and D(0.75, 0.75, 0.75). In the ordered  $\text{Co}_2\text{FeSi}$  crystal, Co atoms occupy two sublattices A, C, and Fe is on sublattice B, while Si atoms fill the sublattice D. Fe and Co atoms cannot be distinguished by TEM, because they have very similar scattering factors ( $f_{\text{Fe}} \approx f_{\text{Co}}$ ). In this approximation the degree of disorder can be described by two order parameters  $\alpha$  and  $\beta$ , which are fractions of Si atoms occupying the Fe(B) and Co(A,C) sites, respectively. Three types of reflections are expected for such a lattice: Fundamental reflections (not sensitive to disorder) and the two kinds of superlattice reflections arising due to long-range order. Figure 1 shows a selected area electron diffraction pattern of the  $\text{Co}_2\text{FeSi}$  film along the  $[01\bar{1}]$  direction. We see a rect-

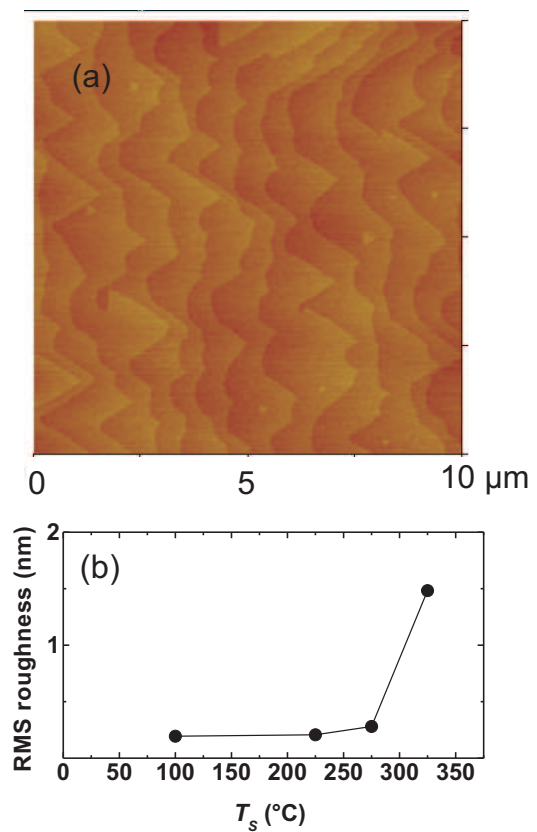


Figure 3. (a) AFM micrograph of the  $\text{Co}_2\text{FeSi}$  surface grown on GaAs(111)B at  $T_S = 100^\circ\text{C}$ . The pattern of the steps is similar to that of a GaAs(111)B surface. Some triangular islands are visible on the broad terraces. (b) Root mean squared (RMS) surface roughness in dependence of the growth temperature of the samples.

angular grid of the fundamental reflections (indexed, see red line) and a less intense hexagonal grid (see black line) of superlattice reflections in the vicinity.

Fundamental reflections are not influenced by disorder. They are given by the rule  $H + K + L = 4n$ , where  $n$  is an integer. One example for a fundamental reflection is 444. The structure amplitude is given by

$$F_{444} = 4(f_{\text{Si}} + f_{\text{Fe}} + 2f_{\text{Co}}), \quad (1)$$

where  $f_{\text{Si}}$ ,  $f_{\text{Fe}}$ ,  $f_{\text{Co}}$  are atomic scattering factors of the respective elements. There are two distinct types of superlattice reflections [15]. Reflections with odd  $H, K, L$  like the 111 reflection are sensitive to both types of disorder (in the Fe(B) and Co(A,C) sublattices with the corresponding order parameters  $\alpha$  and  $\beta$ ), the structure amplitude being

$$F_{111} = 4i(1 - 2\alpha - \beta)(f_{\text{Si}} - f_{\text{Fe}}). \quad (2)$$

Reflections satisfying the condition  $H + K + L = 4n - 2$  are sensitive only to disorder in the Co(A,C) sublattice, an example is 222 with the structure amplitude

$$F_{222} = -4(1 - 2\beta)(f_{\text{Si}} - f_{\text{Co}}). \quad (3)$$

Compared to the fully ordered  $L2_1$  phase, the  $B2$  phase is obtained by a complete mixing between the Fe and the Si atoms in the  $\text{Co}_2\text{FeSi}$  lattice. The Co(A,C) sublattice remains fully ordered in this case and the 222 reflection has still a high intensity, see equation (3).

Figure 2 shows high-resolution x-ray diffraction curves near the 222 diffraction peak of some of the samples investigated. Besides the narrow quasi-forbidden GaAs reflection, the broader  $\text{Co}_2\text{FeSi}$  maximum is pronounced

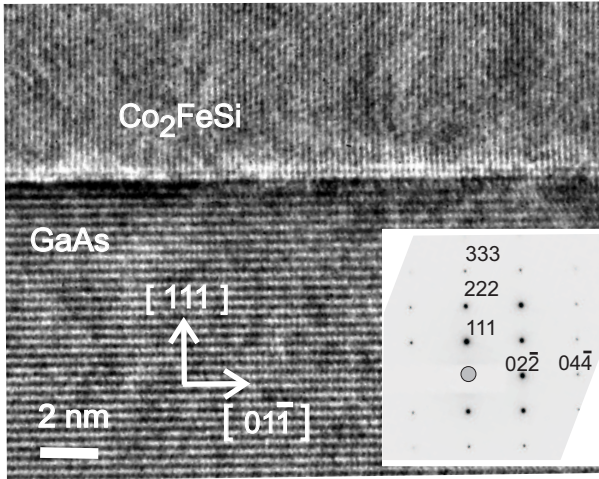


Figure 4. Cross-section HRTEM micrograph (Fourier filtered) along the GaAs  $[2\bar{1}\bar{1}]$  zone axis of a sample grown at  $T_S = 100^\circ\text{C}$  and a corresponding selected area diffraction pattern illustrating the orientational relationship between  $\text{Co}_2\text{FeSi}$  and GaAs. Due to the vanishing misfit between stoichiometric  $\text{Co}_2\text{FeSi}$  and GaAs, their diffraction maxima fully coincide. The interface is smooth.

together with thickness fringes. Those fringes indicate a smooth FM/SC interface and a high quality surface of the film, similar like the results of x-ray reflectivity measurements. The observation of an intense 222 reflection indicates that the Co(A,C) sublattice remains fully ordered and  $\beta \approx 0$ , see equation (3). That means the  $\text{Co}_2\text{FeSi}$  film shows at least a  $B2$  ordering, i.e. the Si atoms can be mixed only with the Fe atoms ( $\alpha > 0$ ) and not with the Co atoms ( $\beta \approx 0$ ). Modifications of the diffraction curves are found for  $T_S = 325^\circ\text{C}$  where the thickness fringes are less pronounced and  $T_S = 425^\circ\text{C}$  where a shift of the peak is found and the thickness fringes vanish.

The morphology of the  $\text{Co}_2\text{FeSi}$  surface after growth at  $T_S = 100^\circ\text{C}$  imaged by atomic force microscopy is excellent, see Fig. 3 (a). For higher growth temperatures a slight deterioration of the surface is found, although the root mean squared (RMS) roughness is limited to values below 0.5 nm for growth temperatures up to  $T_S = 275^\circ\text{C}$ , Fig. 3 (b).

Figure 4 shows a cross-section HRTEM micrograph (Fourier filtered) along the GaAs  $[2\bar{1}\bar{1}]$  zone axis of a sample grown at  $T_S = 100^\circ\text{C}$  and a corresponding selected area diffraction pattern illustrating the cube-on-cube orientational relationship between  $\text{Co}_2\text{FeSi}$  and GaAs. All the diffraction maxima of  $\text{Co}_2\text{FeSi}$  and GaAs overlap fully due to the vanishing misfit between stoichiometric  $\text{Co}_2\text{FeSi}$  and GaAs. For all samples investigated, the orientational relationship  $(111)\text{GaAs} \parallel (111)\text{Co}_2\text{FeSi}$  and  $(110)\text{GaAs} \parallel (110)\text{Co}_2\text{FeSi}$  was established. The interface between the  $\text{Co}_2\text{FeSi}$  film and the GaAs buffer layer is smooth and distributed only over a few monolayers.

Figure 5 is a multi-beam cross-section TEM micrograph at lower magnification along the GaAs  $[01\bar{1}]$  zone axis of a  $\text{Co}_2\text{FeSi}$  film grown on GaAs at  $T_S = 325^\circ\text{C}$ . A large reacted region (lower edge marked by dotted line) is visible below the  $\text{Co}_2\text{FeSi}/\text{GaAs}(111)$  interface. Similar elongated precipitates produced by interfacial reactions were detected by cross-sectional TEM for all samples grown at  $T_S \geq 325^\circ\text{C}$ . Additionally, we found peaks in x-ray diffraction curves caused by the interface reaction products. The precipitates in the samples grown at  $T_S = 325^\circ\text{C}$  are always elongated along the interface and are found only in the immediate vicinity of the interface. They are detected mainly in the GaAs buffer layer, and

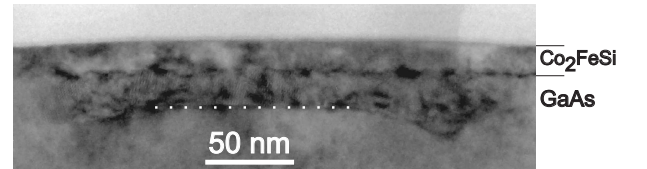


Figure 5. Cross-section multi-beam TEM micrograph along the GaAs  $[01\bar{1}]$  zone axis of a  $\text{Co}_2\text{FeSi}$  film grown on GaAs at  $T_S = 325^\circ\text{C}$ . A large reacted region (lower edge marked by dotted line) is visible below the  $\text{Co}_2\text{FeSi}/\text{GaAs}(111)$  interface.



their predominant boundary is (111). A typical lateral size of these precipitates is  $\approx 100$  nm, whereas the extent of the precipitates perpendicular to the interface is about 10–20 nm, i.e., it may sometimes even reach the film thickness like shown in Fig. 5. The distance between the precipitates is of the order of micrometers. The remaining part of the FM/SC interface between the precipitates is almost perfect. The precipitates in the samples grown at  $T_S = 425^\circ\text{C}$  are even larger and have irregular shapes.

The samples grown at  $T_S = 225^\circ\text{C}$  and at  $T_S = 275^\circ\text{C}$  were still free of interface reactions. For  $T_S = 275^\circ\text{C}$  we could observe some additional phenomena: In the HRTEM micrograph (Fig. 6) a slight modification of the interface (see e.g. the region between the dashed lines) is visible together with the typical inhomogeneities (marked by full lines) of the  $\text{Co}_2\text{FeSi}$  films. The origin of these inhomogeneities will be explained later. Figure 7 shows a comparison of two dark-field micrographs: taken (a) with the 444 fundamental reflection (not sensitive to disorder of the  $\text{Co}_2\text{FeSi}$ ), and (b) with the 111 superlattice reflection (sensitive to disorder).

Let us first consider the GaAs buffer layer: On the GaAs side of the interface we see in (a) and (b) an inhomogeneous stripe caused by strain connected to diffusion of film atoms into the GaAs buffer layer. This diffusion was also detected by SIMS depth profiling, as shown in Fig. 8 for the example of Co in-diffusion. The maximum Co concentration in the uppermost part of the GaAs is almost constant up to a temperature of  $T_S = 275^\circ\text{C}$  and

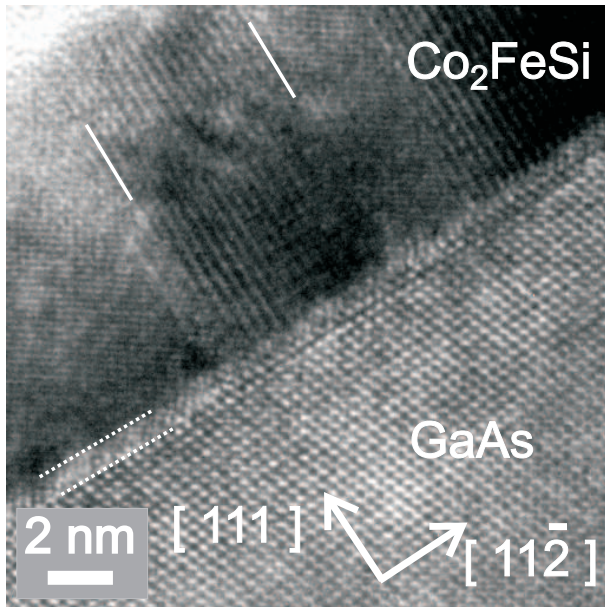


Figure 6. Cross-section HRTEM micrograph along the GaAs  $[01\bar{1}]$  zone axis of a sample grown at  $T_S = 275^\circ\text{C}$ . The FM/SC interface is slightly modified (see region between dashed lines) compared to those of samples grown at lower  $T_S$ . Inhomogeneities of the  $\text{Co}_2\text{FeSi}$  film are visible (marked by full lines).

then increases drastically for the higher growth temperatures. Similar results are obtained for the Fe and Si depth profiles (not shown here). For  $T_S \leq 325^\circ\text{C}$ , a maximum in the Co concentration is found at approximately 20 nm below the interface, which is in good agreement with the observation in Fig. 7. A Co concentration depth profile below a  $\text{Co}_2\text{FeSi}$  layer grown on GaAs(001) at  $T_S = 275^\circ\text{C}$  is also included in Fig. 8. However, the diffusion of Co into the GaAs in this case is strongly enhanced by almost one order of magnitude compared to the films grown on GaAs(111)B at the same  $T_S$  verifying the reduced diffusion activity perpendicular to the (111) plane.

Now let us consider the  $\text{Co}_2\text{FeSi}$  film: The 444 reflection shown in Fig. 7 (a) is a fundamental reflection for the  $\text{Co}_2\text{FeSi}$  lattice, i.e. it is not sensitive to disorder. The disorder-sensitive superlattice 111 reflection is imaged in Fig. 7 (b) [15, 16]. Under the condition, that the TEM micrograph with  $g = 444$  is homogeneous the micrograph taken with  $g = 111$  reveals the spatial distribution of long-range order. It shows brighter areas, that are due to well ordered regions in the film. These ordered regions are not distributed uniformly. Moreover a darker stripe is found near the interface. The image of the  $\text{Co}_2\text{FeSi}$  111 reflection is less homogeneous and less intense than the image of the fundamental  $\text{Co}_2\text{FeSi}$  444 reflection shown in Fig. 7(a). The striking difference in intensity of both reflections (the GaAs intensity should be taken into account as a reference for a comparison) can be explained by their different structure factors, see equations (1) and (2). We estimated from x-ray diffraction results that approximately 25% of the Si atoms left their sublattice (sample grown at  $T_S = 275^\circ\text{C}$ ). For such a disorder the  $\text{Co}_2\text{FeSi}$  444 reflection is expected to be more than 50 times more intense than the  $\text{Co}_2\text{FeSi}$  111 reflection, a value, which seems to be in a reasonable agreement with Fig. 7. The image of the  $\text{Co}_2\text{FeSi}$  222 reflection is more homogeneous than the 111 reflection. This is another hint, that the inhomogeneities are

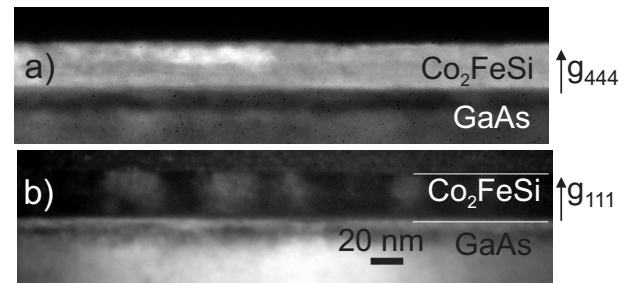


Figure 7. Dark-field cross-section TEM micrographs of the sample grown at  $T_S = 275^\circ\text{C}$ . a) The fundamental  $\text{Co}_2\text{FeSi}$  444 reflection diffracts quite intensively and homogeneously. b) The image of the  $\text{Co}_2\text{FeSi}$  111 superlattice reflection of the same region is less intense and less homogeneous. On the GaAs side of the FM/SC interface both reflections reveal contrasts due to lattice strain connected to diffusion into the GaAs substrate.

caused mainly by mixing of the Fe and the Si atoms in the  $\text{Co}_2\text{FeSi}$ .

In the micrograph shown in Fig. 9, we observe well distinguished grains originating from island growth of  $\text{Co}_2\text{FeSi}$  on  $\text{GaAs}(111)\text{B}$  and the coalescence of those islands. Grains of different orientation produce different interference patterns (phase contrast) in the HRTEM micrograph. Additional tilt or twist of the grains modify these patterns. In the micrograph, one of the grains seems darker and exhibits a modulated phase contrast, which is probably caused by a slight tilt or twist of that grain with respect to its neighbors. In other regions, these modulation stripes are found to be perpendicular to the FM/SC interface pointing to a lateral strain in the grains. So the inhomogeneity in the HRTEM micrograph shown in Fig. 6 resembles the grain structure of the film, which is visible in Fig. 10 on a larger scale. While the GaAs substrate diffracts homogeneously, we see an inhomogeneous contrast in the micrograph of the film, probably caused by residual strain in the different grains. Such a strain could be caused by a local change in stoichiometry, which is always accompanied by a change in the lattice parameter [23]. A change in local stoichiometry may be due to a lateral segregation or stress relaxation near the step edges of the GaAs surface.

Figure 11 shows again a HRTEM micrograph of a sample grown at higher  $T_S = 425^\circ\text{C}$ . Here we see an area with clearly dominant well ordered  $L2_1$  phase in the  $\text{Co}_2\text{FeSi}$  film (honeycomb-like contrast, inset: simulation, performed with the program Electron Microscopy Image Simulation, EMS On Line, <http://cecm.insa-lyon.fr/CIOL/>). Only the region very near to the FM/SC interface consists of the  $B2$  phase (fringe contrast). A comparison of Figures 11 and 6 demonstrates that the micrograph of the sample grown at the lower  $T_S = 275^\circ\text{C}$  exhibits larger areas of fringed contrast patterns with additional inhomogeneities, i.e. the long-range order of the  $\text{Co}_2\text{FeSi}$  lattice is improved for the samples grown at higher  $T_S$ .

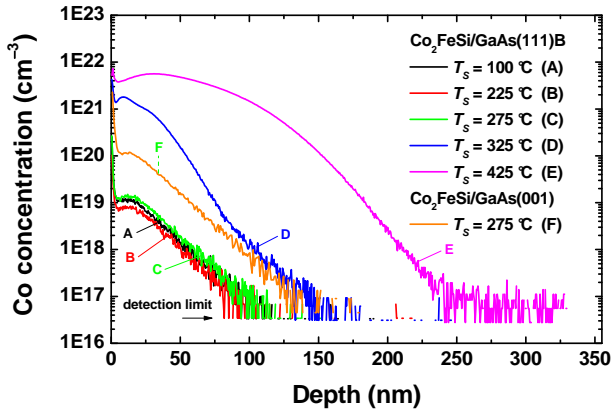


Figure 8. SIMS depth profiles for Co in-diffusion at different growth temperatures of the  $\text{Co}_2\text{FeSi}$  layers.

#### IV. DISCUSSION

At  $T_S \geq 325^\circ\text{C}$  a small amount of plate-like particles are found beneath the FM/SC interface. These particles are obstacles for spin injection. However, the distance between these precipitates is about  $1\ \mu\text{m}$  or more. The remaining part of the FM/SC interface is almost structurally perfect and may still contribute to an effective spin injection into the semiconductor device. This has been recently demonstrated for  $\text{Co}_2\text{FeSi}/(\text{Al,Ga})\text{As}$  spin LEDs grown on  $\text{GaAs}(001)$  substrates, where a higher spin injection efficiency was obtained inspite of the presence of precipitates due to the high  $T_S$  of the spin injector layer [10]. The morphology of the reacted regions near the (111) interface is clearly different from the appearance of the precipitates found in samples grown on  $\text{GaAs}(001)$  [14]. In our case the precipitates are larger and more flattened along the (111) interface. Therefore (111) boundaries seem to act as barriers for diffusion-driven precipitate formation.

Our samples grown at  $T_S = 275^\circ\text{C}$  were still free of interface reactions, although a modification of the interface was found, see Fig. 6. MBE growth of  $\text{Co}_2\text{FeSi}$  on  $\text{GaAs}(001)$  resulted in an interface reaction at the lower  $T_S = 250^\circ\text{C}$ , while a modification of the interface took already place at  $T_S = 200^\circ\text{C}$ , cf. [14, 23]. So, the  $\text{Co}_2\text{FeSi}/\text{GaAs}(111)\text{B}$  hybrid structures are stable at temperatures 75 K higher than  $\text{Co}_2\text{FeSi}/\text{GaAs}(001)$  structures in agreement with our expectation mentioned in the introduction.

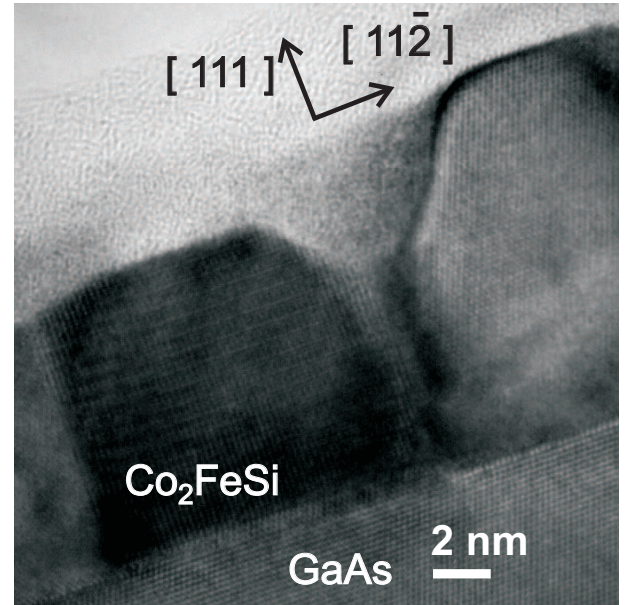


Figure 9. Cross-section HRTEM micrograph along the  $\text{GaAs}[01\bar{1}]$  zone axis of a sample grown at  $T_S = 425^\circ\text{C}$ . Different grains can be distinguished clearly and for one grain a modulated contrast pattern is observed. Obviously the grains were formed after coalescence of islands. The shape of the former islands is visible from the shape of the  $\text{Co}_2\text{FeSi}$  surface.

Despite a vanishing misfit between the  $\text{Co}_2\text{FeSi}$  film and the GaAs buffer layer, the observed formation of grains in the film is evidence for three-dimensional island growth during the first stage of heteroepitaxy of  $\text{Co}_2\text{FeSi}$  on GaAs(111)B before a continuous film is formed. Such island growth is caused by the higher surface tension of the metal compared to the semiconductor substrate. The surface tension of  $\text{Co}_2\text{FeSi}$  is similar to that of  $\text{Fe}_3\text{Si}$ , for which the Volmer-Weber growth mode was observed on GaAs(001) earlier using *in-situ* x-ray diffraction [21, 22]. Indeed the difference of the surface tension  $\Delta\gamma_1$  of  $\text{Fe}_3\text{Si}$  and  $\text{Co}_2\text{FeSi}$  should be small compared to the difference  $\Delta\gamma_2$  of GaAs and  $\text{Co}_2\text{FeSi}$  ( $\Delta\gamma_1 \ll \Delta\gamma_2$ ) leading us to the expectation of an island growth mode of  $\text{Co}_2\text{FeSi}$  on GaAs(111)B. However, *in-situ* RHEED measurements did not detect a roughening of the surface indicating relatively large and very flat islands. Our growth rate one monolayer in three minutes is very near to a simulated kinetic optimum of Volmer-Weber growth with a resulting RMS surface roughness of less than one monolayer during all stages of the growth, see kinetic Monte Carlo simulations in [21].

We show by HRTEM that the long-range order of the  $\text{Co}_2\text{FeSi}$  lattice improves with increasing  $T_S$ . However, near the FM/SC interface we often find some disordering (B2 phase) especially at the higher  $T_S$ . In addition, the lateral homogeneity of ordering can be imaged by dark-field TEM using superlattice reflections e.g. 111 or 222, provided, the image of the fundamental reflection 444 is more homogeneous in the same area. In our case the spatial distribution of the long-range order in

Fig. 7(b) is similar to the distribution of grains shown in Figs. 9 and 10. The origin of these grainy inhomogeneities in the long-range order probably lies in a segregation at step edges or a local strain relaxation of the the  $\text{Co}_2\text{FeSi}$  film (without formation of misfit dislocations) via non-stoichiometry (with a formation and movement of point defects) leading to a local change in the lattice. In one way or the other neighboring grains would have a slightly different lattice parameter. No extended defects are needed for these inhomogeneities. A change in stoichiometry of the the  $\text{Co}_2\text{FeSi}$  film could arise as a consequence of the diffusion into the GaAs buffer layer as well. Obviously inhomogeneity of the stoichiometry is directly connected to inhomogeneity of long-range ordering. During the epitaxial growth the islands nucleate independently and randomly on the GaAs surface, grow and eventually coalesce. In this way the local growth conditions in each of the grains influence long-range order in this grain, e.g. due to different sticking of the  $\text{Co}_2\text{FeSi}$  film atoms at step edges or simply due to a slight change in stoichiometry driven by inhomogeneity of local mismatch.

## V. SUMMARY

$\text{Co}_2\text{FeSi}$  films on GaAs(111)B grow in the Volmer-Weber island growth mode, contain the ordered  $L2_1$  phase, and have a stable interface up to  $T_S = 275^\circ\text{C}$ , a growth temperature which is 75 K higher than the temperature guaranteeing a stable interface during growth

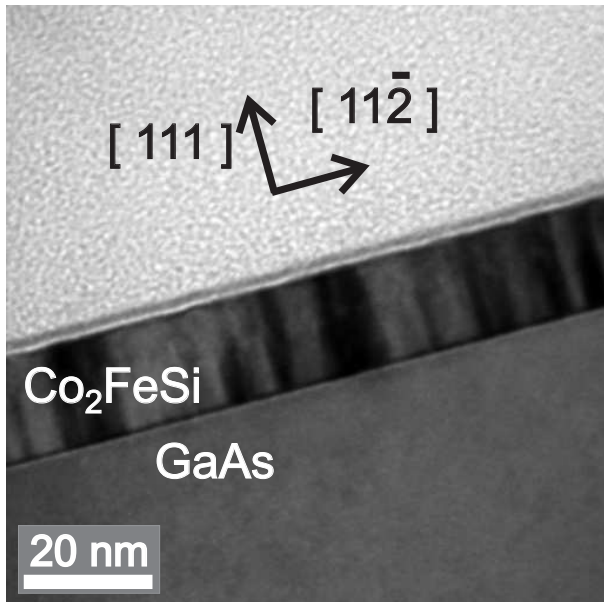


Figure 10. Cross-section multi-beam TEM micrograph at lower magnification along the GaAs  $[01\bar{1}]$  zone axis of a sample grown at  $T_S = 100^\circ\text{C}$ . Different grains can be distinguished due to changing contrast in the micrograph. The GaAs substrate diffracts homogeneously.

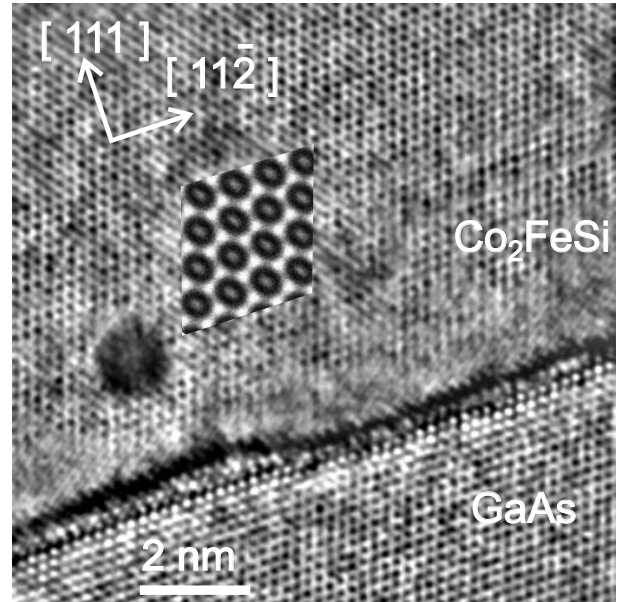


Figure 11. Cross-section HRTEM micrograph (Fourier filtered) along the GaAs  $[01\bar{1}]$  zone axis of a sample grown at  $T_S = 425^\circ\text{C}$ . Here the dominant  $L2_1$  phase of  $\text{Co}_2\text{FeSi}$  is observed more far from the interface (inset: simulation), whereas the B2 phase (fringed contrast) is seen near the interface.



on GaAs(001). The distribution of long-range order in the  $\text{Co}_2\text{FeSi}$  films can be characterized by comparison of the dark-field TEM images taken in a homogeneous fundamental reflection and an inhomogeneous superlattice reflection. The spatial inhomogeneities in the long-range order resemble the grainy structure of the  $\text{Co}_2\text{FeSi}$  film. They are arising during the growth of the islands and their coalescence via a local change in stoichiometry, which can lead to a relaxation of local strain without formation of extended defects.

## VI. ACKNOWLEDGEMENT

The authors thank Hans-Peter Schönherr for his support during the MBE growth, Doreen Steffen for sample preparation, Astrid Pfeiffer for help in the laboratory, Esperanza Luna and Vladimir Kaganer for valuable support and helpful discussion.

- 
- [1] C. Felser and B. Hillebrands, J. Phys. D: Appl. Phys. **42**, 080301 (2009).
  - [2] G. A. Prinz, Science **282**, 1660 (1998).
  - [3] A. Fert, Thin Solid Films **517**, 2 (2008).
  - [4] I. Zutić, J. Fabian, and S. D. Sarma, Rev. of Mod. Phys. **76**, 323 (2004).
  - [5] S. Wurmehl, G. H. Fecher, H. C. Kandpal, V. Ksenofontov, C. Felser, H.-J. Lin, and J. Morais, Phys. Rev. B **72**, 184434 (2005).
  - [6] S. Wurmehl, G. H. Fecher, H. C. Kandpal, V. Ksenofontov, C. Felser, and H.-J. Lin, Appl. Phys. Lett. **88**, 032503 (2006).
  - [7] Y. Ohno, D. K. Young, B. Beschoten, F. Matsukura, H. Ohno, and D. D. Awschalom, Nature **402**, 790 (1999).
  - [8] H. J. Zhu, M. Ramsteiner, H. Kostial, M. Wassermeier, H.-P. Schönherr, and K. H. Ploog, Phys. Rev. Lett. **87**, 016601 (2001).
  - [9] A. T. Hanbicki, B. T. Jonker, G. Itskos, G. Kioussoglou, and A. Petrou, Appl. Phys. Lett. **80**, 1240 (2002).
  - [10] M. Ramsteiner, O. Brandt, T. Flissikowski, H. T. Grahn, M. Hashimoto, J. Herfort, and H. Kostial, Phys. Rev. B **78**, 121303 (2008).
  - [11] S. Sugahara and M. Tanaka, Appl. Phys. Lett. **84**, 2307 (2004).
  - [12] M. Kallmayer, H. J. Elmers, B. Balke, S. Wurmehl, F. Emmerling, G. H. Fecher, and C. Felser, J. Phys. D: Appl. Phys. **39**, 786 (2006).
  - [13] J. J. Attema, G. A. de Wijs, and R. A. de Groot, J. Phys. D: Appl. Phys. **39**, 793 (2006).
  - [14] M. Hashimoto, J. Herfort, A. Trampert, H.-P. Schönherr, and K. H. Ploog, J. Phys. D: Appl. Phys. **40**, 1631 (2007).
  - [15] V. Niculescu, K. Raj, J. I. Budnick, T. J. Burch, W. A. Hines, and A. H. Menotti, Phys. Rev. B **14**, 4160 (1976).
  - [16] V. Niculescu, J. I. Budnick, W. A. Hines, K. Raj, S. Pickard, and S. Skalski, Phys. Rev. B **19**, 452 (1979).
  - [17] B. Jenichen, V. M. Kaganer, J. Herfort, D. K. Satapathy, H. P. Schönherr, W. Braun, and K. H. Ploog, Phys. Rev. B **72**, 075329 (2005).
  - [18] Y. Takamura, R. Nakane, and S. Sugahara, J. Appl. Phys. **105**, 07109 (2009).
  - [19] E. Bauer, Z. Kristallographie **110**, 372 (1958).
  - [20] J. Y. Tsao, *Materials Fundamentals of Molecular Beam Epitaxy* (Academic Press, Inc., San Diego, CA, 1992).
  - [21] V. M. Kaganer, B. Jenichen, R. Shayduk, W. Braun, and H. Riechert, Phys. Rev. Lett. **102**, 016103 (2009).
  - [22] B. Jenichen, V. M. Kaganer, R. Shayduk, W. Braun, and A. Trampert, Phys. Stat. Sol. A **206**, 1740 (2009).
  - [23] M. Hashimoto, J. Herfort, H.-P. Schönherr, and K. H. Ploog, Appl. Phys. Lett. **87**, 102506 (2005).
  - [24] M. Hashimoto, J. Herfort, H.-P. Schönherr, and K. H. Ploog, J. Appl. Phys. **98**, 104902 (2005).